

Zig-zag sampling for discrete structures and non-reversible phylogenetic MCMC

Jere Koskela

`j.koskela@warwick.ac.uk`

Department of Statistics

University of Warwick

Coventry CV4 7AL, UK

August 19, 2022

Abstract

We construct zig-zag processes targeting posterior distributions arising in genetics from the Kingman coalescent and two popular models of mutation. We show that the zig-zag process can lead to efficiency gains of up to several orders of magnitude over classical Metropolis–Hastings algorithms, and that it is well suited to parallel computation for coalescent models. Our construction is based on embedding discrete variables into a continuous space; a technique previously employed by coalescent Hamiltonian Monte Carlo algorithms which suffer from implementationally and analytically complex boundary crossings. We demonstrate that the continuous-time zig-zag process avoids similar complications.

Keywords: Bayesian statistics; coalescent; data augmentation; piecewise-deterministic Markov process

1 Introduction

The zig-zag process is a non-reversible, piecewise deterministic Markov process introduced by [BR17, BFR19b] for continuous-time MCMC. It has several advantages over reversible methods such as Metropolis–Hastings [Has70] and Gibbs sampling [GS90]: it avoids diffusive backtracking which slows their mixing, and is rejection-free so that no computation is wasted on rejected moves.

In brief, a zig-zag process $\mathbf{Z} \equiv (\mathbf{Z}_t)_{t \geq 0} \equiv (\mathbf{X}_t, \mathbf{v}_t)_{t \geq 0}$ with velocity $\mathbf{v}_t \in V \subseteq \mathbb{R}^d$ targeting the \mathbf{X}_t -marginal probability density $\pi(\mathbf{x})$ defined on $X \subseteq \mathbb{R}^d$ has generator

$$Lf(\mathbf{x}, \mathbf{v}) = \sum_{i=1}^d v_i \partial_i f(\mathbf{x}, \mathbf{v}) + \sum_{i=1}^d \lambda_i(\mathbf{x}, \mathbf{v})(f(\mathbf{x}, F_i \mathbf{v}) - f(\mathbf{x}, \mathbf{v})),$$

where ∂_i is the x_i -partial derivative, and F_i flips the sign of v_i . The flip rates

$$\lambda_i(\mathbf{x}, \mathbf{v}) := (-v_i \partial_i \log(\pi(\mathbf{x})))^+$$

ensure that $\pi(\mathbf{x})/2^d$ a stationary distribution of \mathbf{Z} [BFR19b, Theorem 2.2]. In words, the coordinates of \mathbf{X}_t move at constant velocities \mathbf{v}_t until a flip at coordinate i , when the velocity of the i th coordinate changes sign.

To date, the zig-zag processes have been applied to targets such as the Curie–Weiss model [BR17] and logistic regression [BFR19b], whose state spaces have simple geometric structures with natural notions of direction and velocity. Discrete variables have only been considered in

cases with a natural ordering, such as model selection [CFS20, GD20]. We construct a zig-zag process for the coalescent [Kin82]: a tree-valued target with continuous branch lengths, discrete tree topologies with no natural partial order, and no canonical geometric structure. This is done by embedding branch lengths and topologies into a single continuous space following similar strategies for Hamiltonian Monte Carlo (HMC) [DBZM17, NDL20] and zig-zag processes for variable selection [CFS20].

Existing MCMC algorithms for coalescents tend to mix slowly because it is difficult to design proposal distributions which combine efficient exploration with a high acceptance rate [MV05, HDPD08, LVH⁺08]. Workarounds consist of empirical searches for efficient proposals [HD12, ASR16] or Metropolis-coupled MCMC [Gey92]. The former does not scale to problems for which empirical optimization is infeasible. The latter helps mixing between modes, but does not overcome low acceptance rates or the backtracking behavior of reversible MCMC.

HMC [Nea10] is a variant of Metropolis–Hastings that has some similarities with the zig-zag process. It augments the state space with momentum and uses Hamiltonian dynamics to propose large steps which are accepted with high probability, though they are not rejection-free. Like the zig-zag process, HMC requires gradient information and a suitable geometric embedding of the target. [DBZM17] provided these for the coalescent and the finite sites mutation model [JC69] using an orthant complex construction of phylogenetic tree space [BHV01]. Our work differs from the method of [DBZM17] in three ways:

1. We replace the embedding of [BHV01] with the τ -space of [GD16], which is better suited to ultrametric coalescent trees.
2. The zig-zag process is readily implementable on τ -space via Poisson thinning without a numerical integrator such as *leap-prog* [DBZM17, Algorithm 1].
3. The zig-zag process has simple boundary behavior between orthants and does not require boundary smoothing [DBZM17, Section 3.3], chiefly because discontinuous gradients are easier to handle with continuous rather than discretized paths.

We demonstrate that the zig-zag process mixes over the space of latent trees efficiently. Our construction is not specific to the coalescent, and can be adapted to other models provided a suitable embedding of discrete variables into continuous space is available.

The rest of the paper is structured as follows. Section 2 recapitulates the coalescent and the τ -space embedding. Sections 3 and 4 recall the popular infinite and finite sites models of mutation, derive zig-zag processes for each, and demonstrate their performance via simulation studies. Section 5 outlines how embeddings into continuous space can be used to construct zig-zag processes for general targets with discrete components, and Section 6 concludes with a discussion. The algorithms and data sets used to conduct the simulation studies in Sections 3 and 4 are available at <https://github.com/JereKoskela/tree-zig-zag>.

2 The coalescent and a geometric embedding

An ultrametric binary tree with n labeled leaves is a rooted binary tree in which each leaf is an equal graph distance away from the root. We follow [GD16] and encode such a tree with leaf labels $\{1, \dots, n\}$ as the pair (E_n, \mathbf{t}_n) , where E_n is a ranked topology and $\mathbf{t}_n \in \mathbb{R}_+^{n-1}$. The continuous variables \mathbf{t}_n do not represent branch lengths directly, but rather encode times between mergers. The time from the leaves to the first merger is t_1 , and subsequent t_i variables are times between successive mergers. The ranked topology E_n specifies which nodes merge in each event. It is an $(n - 1)$ -tuple of pairs of labels, where the i th pair specifies the two child nodes of the i th merger. Non-leaf nodes are labeled by the leaves they subtend. For example, the ranked

topology

$$E_4 = (E_{4,1}, E_{4,2}, E_{4,3}) := (\{1, 2\}, \{\{1, 2\}, 3\}, \{\{1, 2, 3\}, 4\})$$

encodes the four leaf caterpillar tree depicted in Figures 3 and 7 with nodes labeled left to right. We order the two entries of $E_{n,i}$ by their least element for definiteness.

The coalescent [Kin82] is a seminal model for the genetic ancestry of samples from large populations. Under the coalescent, a tree (E_n, \mathbf{t}_n) has probability density

$$\pi(E_n, \mathbf{t}_n) d\mathbf{t}_n := \exp\left(-\sum_{i=1}^{n-1} \binom{n+1-i}{2} t_i\right) d\mathbf{t}_n,$$

which arises as the law of a tree constructed by starting a lineage from each leaf, and merging each pair of lineages at rate 1 until the most recent common ancestor (MRCA) is reached. The success of the coalescent is due to robustness: distributions of ancestries of a large class of individual-based models converge to the coalescent in the infinite population limit under suitable rescalings of time. For details, see e.g. [Wak09].

We define a family of swap operators $\{s_i\}_{i=2}^{n-2}$ for E_n such that $E_{n,i-1} \notin E_{n,i}$ via

$$s_i(E_n) := (E'_{n,1}, \dots, E'_{n,n-1}) \text{ where } E'_{n,k} := \begin{cases} E_{n,k} & \text{for } k < i-1 \text{ or } k > i, \\ E_{n,i} & \text{for } k = i-1, \\ E_{n,i-1} & \text{for } k = i. \end{cases}$$

In words, s_i swaps the order of the $(i-1)$ th and i th mergers. We also define families of pivot operators $\{p_i^\downarrow\}_{i=2}^{n-1}$ and $\{p_i^\uparrow\}_{i=2}^{n-1}$ for E_n with $E_{n,i-1} \in E_{n,i}$ as

$$p_i^\downarrow(E_n) := (E'_{n,1}, \dots, E'_{n,n-1}) \text{ with } E'_{n,k} := \begin{cases} E_{n,k} & \text{for } k < i-1 \text{ or } k > i, \\ \{E_{n,i-1}^\downarrow, E_{n,i}^s\} & \text{for } k = i-1, \\ \{E_{n,i-1}^\uparrow, E_{n,i-1}\} & \text{for } k = i, \end{cases} \quad (1)$$

where $E_{n,i}^\uparrow$ (resp. $E_{n,i}^\downarrow$) is the entry of $E_{n,i}$ with the higher (resp. lower) least element, and $E_{n,i}^s$ is the *sibling*: the entry of $E_{n,i}$ that is not $E_{n,i-1}$. Pivot p_i^\uparrow is defined by interchanging \downarrow and \uparrow in (1). The pivots are the two nearest neighbor interchanges between the i th merger and the merger involving its nearest child. Figure 1 illustrates all three operators.

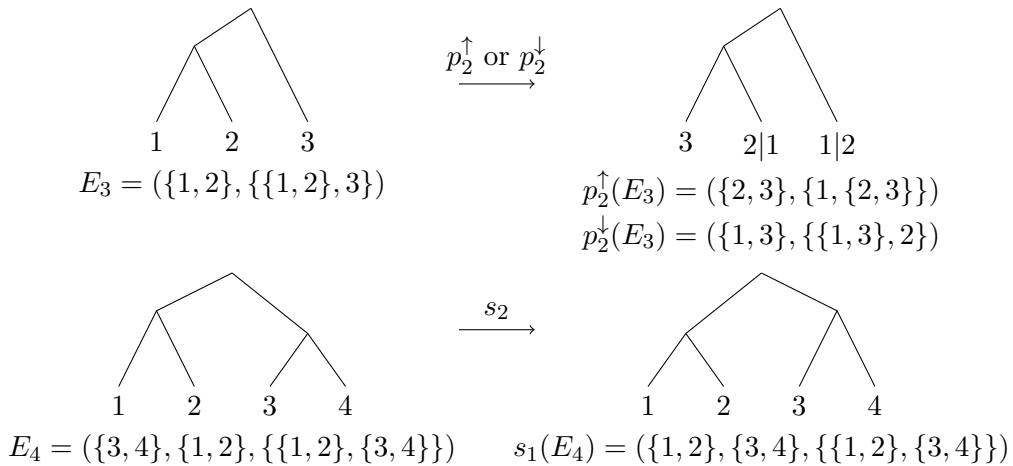


Figure 1: Operators p_2^\downarrow , p_2^\uparrow , and s_2 . Label $x|y$ means either x or y depending on the pivot.

Next we describe τ -space, which gives a geometric structure to the set of pairs (E_n, \mathbf{t}_n) . For fixed E_n , the space of \mathbf{t}_n -vectors is the orthant \mathbb{R}_+^{n-1} . Each boundary point with $t_i = 0$ corresponds to a degenerate tree in which one of three things happens:

1. The two leaves of $E_{n,1}$ merge at time 0 if $i = 1$.
2. There are two simultaneous mergers if $E_{n,i-1} \notin E_{n,i}$.
3. There is a simultaneous merger of three lineages if $E_{n,i-1} \in E_{n,i}$.

Type 1 boundaries are boundaries of the whole τ -space. At type 2 boundaries we glue together the orthants corresponding to the two ranked topologies separated by an s_i -step. Continuous trajectories crossing the boundary move from one ranked topology to the other. At type 3 boundaries we glue together the three orthants which resolve the triple merger into two binary mergers, which differ by a p_i^\downarrow or p_i^\uparrow -step. A continuous trajectory that crosses the boundary visits the tree containing the triple merger. Figure 2 illustrates the τ -space with three leaves, and type 2 boundary in a general τ -space. A further example with five leaves is depicted in [GD16, Figure 2], and the \mathbf{t}_n variables are illustrated in Figures 3 and 7 in Sections 3 and 4.

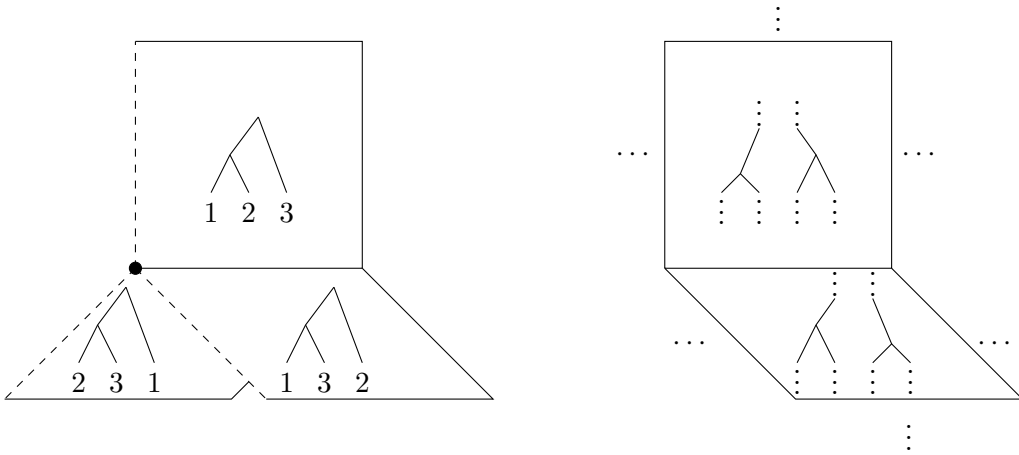


Figure 2: (Left) τ -space with $n = 3$. Each square is a copy of \mathbb{R}_+^2 associated with the depicted topology. The coordinates $(t_1, t_2) \in \mathbb{R}_+^2$ are the time of the first merger and the time between the first and second merger, respectively. The dot denotes the origin, and the line on which all three orthants intersect is a type 3 boundary consisting of trees in which all three leaves merge simultaneously at time t_1 . The dashed edges are type 1 boundaries. (Right) A segment of τ -space depicting a type 2 boundary, in which each square represents \mathbb{R}_+^{n-1} . Only the two orthants adjacent to the boundary are shown.

This embedding enables us to construct a zig-zag process with paths driven by $(n - 1)$ velocities $\mathbf{v}_n := (v_1, \dots, v_{n-1})$, corresponding to the holding times \mathbf{t}_n . The process explores ranked topologies via boundary crossings. For more details on τ -space, e.g. existence and uniqueness of geodesics and Fréchet means, we refer to [GD16].

3 The infinite sites model

The infinite sites model [Wat75] associates the MRCA with $(0, 1)$. Mutations accrue along branches of the tree at rate $\theta/2$, and each is labeled with a $U(0, 1)$ -distributed location. The type of a leaf consist of the mutations along branches separating it from the MRCA. Because all mutations are visible in the leaves and a mutation at a given location can only arise once, an observed pattern of mutations restricts the unobserved tree to topologies consistent with the mutations. We add the mutation rate θ into the state space by introducing a velocity v_θ , flip rate λ_θ , and a prior density $\pi_0(\theta)$ on \mathbb{R}_+ . A realization of an infinite sites coalescent tree and associated data set is depicted in Figure 3.

is at least one mutation in total. See Proposition 1 for a proof of their inaccessibility. The parameter $c > 0$ ensures that, when the current process time is t , inaccessible boundaries cannot be hit on $[t, t + T]$, and at most one accessible boundary can be reached. We found $c = 4$ gave good performance across our tests in Sections 3 and 4. A larger value results in tighter bounds on (3) and (4), but wastes more computation as $t + T$ is hit more often before an accepted velocity flip.

On time interval $[t, t + T]$, flip rates (3) and (4) are bounded above by constant rates

$$\lambda_i^* := \left[v_i \left(\frac{(n+1-i)(n+\theta+(v_\theta T)^\pm - i)}{2} - \sum_{\gamma \in F_n: t_i \in \gamma} \frac{m_\gamma}{l_\gamma + (v_\gamma T)^\pm} \right) \right]^+,$$

$$\lambda_\theta^* := \left[v_\theta \left(\sum_{i=1}^{n-1} \frac{n+1-i}{2} [t_i + (v_i T)^\pm] - \frac{1}{\theta + v_\theta T} \sum_{\gamma \in F_n} m_\gamma - \inf_{s \in [0, T]} \{\partial_\theta \log(\pi_0(\theta + v_\theta s))\} \right) \right]^+,$$

where, for each λ_i^* , $i \in \{1, \dots, n-1, \theta\}$, $(x)^\pm := (x)^+$ if $v_i > 0$ and $(x)^\pm := (x)^- := \min\{x, 0\}$ if $v_i < 0$. Algorithms 1 and 2 detail how to simulate holding times and flips by thinning these rates.

Algorithm 1 Simulation of zig-zag process targeting π

Require: $E_n, \mathbf{t}_n, \theta, \mathbf{v}_n, v_\theta, t_{\text{end}}, c, K$

```

1: Set  $t \leftarrow 0$ 
2: while  $t < t_{\text{end}}$  do
3:   Set  $\tau \leftarrow K$  and  $I \leftarrow 0$   $\triangleright K \in (0, \infty)$  is a default increment if all  $v_i > 0$ .
4:   for  $i \in \{1, \dots, n-1, \theta\}$  do  $\triangleright t_\theta := \theta$  for brevity.
5:     if  $v_i < 0$  then
6:       Set  $d \leftarrow 1$  and  $J \leftarrow i$ 
7:       if  $(i \in \{1, \theta\}$  or  $E_{n,i-1} \in E_{n,i})$  and  $m_{\gamma(E_{n,i})} > 0$  then
8:         Set  $d \leftarrow 1 + c$  and  $J \leftarrow 0$   $\triangleright I = 0 \Rightarrow$  localization refresh with no flip.
9:         if  $-t_i/(d \times v_i) < \tau$  then
10:          Set  $\tau \leftarrow -t_i/(d \times v_i)$  and  $I \leftarrow J$ 
11:       for  $i \in \{1, \dots, n-1, \theta\}$  do  $\triangleright t_\theta := \theta$  as above.
12:         Sample  $\rho \leftarrow \text{NextFlip}(E_n, \mathbf{t}_n, \theta, \mathbf{v}_n, v_\theta; i, \tau)$ 
13:         if  $\rho < \tau$  then
14:           Set  $\tau \leftarrow \rho$  and  $I \leftarrow i$ 
15:       Set  $t \leftarrow t + \tau$ 
16:       for  $i \in \{1, \dots, n-1, \theta\}$  do  $\triangleright t_\theta := \theta$  as above.
17:         Set  $t_i \leftarrow t_i + v_i \tau$ 
18:       if  $I \neq 0$  then
19:         Set  $v_I \leftarrow -v_I$ 
20:       if  $I \notin \{0, 1, \theta\}$  and  $t_I = 0$  then
21:         if  $E_{n,I-1} \in E_{n,I}$  then
22:           Sample  $Y \sim U(\{\uparrow, \downarrow\})$ 
23:           Set  $E_n \leftarrow p_I^Y(E_n)$ 
24:         else
25:           Set  $E_n \leftarrow s_I(E_n)$ 
26: end while

```

The for-loop on lines 4–10 of Algorithm 1 implements the time localization and ensures that a time step cannot cause negative entries in \mathbf{t}_n . The distribution of the increment τ thus has an atom at the value determined by lines 4–10, signifying either a boundary crossing or a need to

recompute the time localization and rates $\{\lambda_i^* : i \in \{1, \dots, n-1, \theta\}\}$. However, the continuous-time motion of the trajectory is not interrupted in either case; see also [BBCD⁺18, Section 2.2].

Iterations of the outer while-loop of Algorithm 1 flip a velocity for one of two reasons: a flip event occurs or a boundary is hit. In the former case the reason for the flip is clear by construction. In the latter, a trajectory arriving at a boundary must have $v_i < 0$ for the corresponding velocity. After crossing, the trajectory moves into the interior of an adjacent orthant, which corresponds to $v_i > 0$ in its local coordinates.

Algorithm 2 NextFlip

Require: $E_n, \mathbf{t}_n, \theta, \mathbf{v}_n, v_\theta, i, \tau$

```

1: Set  $\rho \leftarrow 0$ 
2: repeat
3:   Sample  $s \sim \text{Exp}(\lambda_i^*)$ 
4:   Set  $\rho \leftarrow \rho + s$ 
5:   if  $\rho < \tau$  then
6:     Set  $\alpha \leftarrow \lambda_i(E_n, \mathbf{t}_n + \mathbf{v}_n \rho, \theta + v_\theta \rho; \mathbf{v}_n, v_\theta) / \lambda_i^*$ 
7:   else ▷ Guaranteed to not be the shortest waiting time.
8:     Set  $\alpha \leftarrow 1$ 
9:   Sample  $U \sim U(0, 1)$ 
10: until  $U < \alpha$ 
11: return  $\rho$ 

```

Proposition 1. *Suppose that the initial ranked topology E_n is compatible with the observed pattern of mutations, that the initial holding times \mathbf{t}_n have a joint density on \mathbb{R}_+^{n-1} , and that $\partial_\theta \log(\pi_0(\theta))$ is bounded on compact subsets of $[0, \infty)$. Then the distribution proportional to (2) is stationary under the dynamics simulated by Algorithm 1.*

Proof. We begin by restricting the set of states by showing that corners in which more than one boundary intersect are never hit, and that boundaries of orthants incompatible with observed mutations are inaccessible (equivalently, edges with mutations cannot vanish).

The joint density of initial holding times ensures that the initial condition satisfies $\mathbb{P}(t_i/v_i = t_j/v_j) = 0$ for if $i \neq j$. Hence, the Poisson construction of the zig-zag dynamics ensures that two edges cannot vanish simultaneously, and an edge must span only one holding time for a positive length of time before shrinking to length 0.

Fix an edge $\delta \in F_n$ with $m_\delta > 0$, and suppose it spans one holding time t_q with velocity $v_q < 0$ (without loss of generality $v_q = -1$) and flip rate λ_q . Suppose hitting the $t_q = 0$ boundary will be the next event if no flips occur, which must be true for some length of time before $t_q = 0$ is hit. Then, for sufficiently small t_q we have

$$\lambda_q(E_n, \mathbf{t}_n, \theta; \mathbf{v}_n, v_\theta) = \left(\frac{m_\delta}{t_q} + \sum_{\gamma \neq \delta: t_q \in \gamma} \frac{m_\gamma}{l_\gamma} - \frac{(n+1-q)(n+\theta-q)}{2} \right),$$

and the corresponding survival function for $0 < \tau < t_q$ is

$$\begin{aligned} & \exp \left(- \int_0^\tau \left(\frac{m_\delta}{t_q - s} - \sum_{\gamma \neq \delta: t_q \in \gamma} \frac{m_\gamma}{l_\gamma + v_\gamma s} + \frac{(n+1-q)(n+\theta+v_\theta s - q)}{2} \right) ds \right) \\ &= \left(\frac{t_q - \tau}{t_q} \right)^{m_\delta} \exp \left(- \frac{(n+1-q)\tau}{2} \left(n + \theta - q + \frac{v_\theta \tau}{2} \right) \right) \prod_{\gamma \neq \delta: t_q \in \gamma} \left(1 + \frac{v_\gamma \tau}{l_\gamma} \right)^{\frac{m_\gamma}{v_\gamma}}. \end{aligned}$$

Letting $\tau \rightarrow t_q$ shows that the probability of a flip of v_q before time t_q is 1. An analogous argument shows that $\theta = 0$ is inaccessible if there is at least one mutation because boundedness of $\partial_\theta \log(\pi_0(\theta))$ means (4) diverges at $\theta = 0$ when $v_\theta < 0$. If there are no mutations then $\theta = 0$ is an accessible, reflecting boundary.

Consider now a point $(E_n, \mathbf{t}_n, \theta)$ in the interior of an orthant E_n consistent with observed mutations. The local dynamics of Algorithm 1 at such a point coincide with the standard zig-zag algorithm, and hence π given by (2) satisfies the Fokker–Planck equation,

$$\begin{aligned} & \sum_{i=1}^{n-1} [\lambda_i(E_n, \mathbf{t}_n, \theta; F_i \mathbf{v}) \pi(E_n, \mathbf{t}_n, \theta) - \lambda_i(E_n, \mathbf{t}_n, \theta; \mathbf{v}) \pi(E_n, \mathbf{t}_n, \theta) - v_i \partial_i \pi(E_n, \mathbf{t}_n, \theta)] \\ & + \lambda_\theta(E_n, \mathbf{t}_n, \theta; F_\theta \mathbf{v}) \pi(E_n, \mathbf{t}_n, \theta) - \lambda_\theta(E_n, \mathbf{t}_n, \theta; \mathbf{v}) \pi(E_n, \mathbf{t}_n, \theta) - v_\theta \partial_\theta \pi(E_n, \mathbf{t}_n, \theta) = 0, \end{aligned} \quad (5)$$

at these points by construction [FBPR18, Section 2.2.2].

Equation (5) is solved by any constant multiple of π , so it remains to check that boundary crossings conserve probability mass within orthants. To that end, it will be convenient to extend the definition of π to include velocities via $\pi(E_n, \mathbf{t}_n, \theta, \mathbf{v}_n, v_\theta) := \pi(E_n, \mathbf{t}_n, \theta)/2^n$.

Consider a point $(E_n, \mathbf{t}_n, \theta, \mathbf{v}_n, v_\theta)$ with $t_i = 0+$ for one $i \in \{2, \dots, n-2\}$ on a type 2 boundary, and with $v_i < 0$. From initial distribution π , the probability flow from $(E_n, \mathbf{t}_n, \theta, \mathbf{v}_n, v_\theta)$ into $(s_i(E_n), \mathbf{t}_n, \theta, F_i \mathbf{v}_n, v_\theta)$ is $|v_i| \pi(E_n, \mathbf{t}_n, \theta, \mathbf{v}_n, v_\theta)$. Similarly, the flow from $(s_i(E_n), \mathbf{t}_n, \theta, \mathbf{v}_n, v_\theta)$ into $(E_n, \mathbf{t}_n, \theta, F_i \mathbf{v}_n, v_\theta)$ is $|v_i| \pi(s_i(E_n), \mathbf{t}_n, \theta, \mathbf{v}_n, v_\theta)$, and the net flux in the $(E_n, \mathbf{t}_n, \theta)$ -marginal is zero by continuity of π and the fact that π is uniform over velocities. The same equilibrium holds at all non-corner points on all type 2 boundaries.

The net flux across type 3 boundaries is similar: consider a point $(E_n, \mathbf{t}_n, \theta, \mathbf{v}_n, v_\theta)$ with $t_i = 0+$ for one $i \in \{2, \dots, n-1\}$ on a type 3 boundary adjacent to three orthants: E_n , $p_i^\uparrow(E_n)$, and $p_i^\downarrow(E_n)$, and with $v_i < 0$. The flow into $(E_n, \mathbf{t}_n, \theta, F_i \mathbf{v}_n, v_\theta)$ from $(p_i^\uparrow(E_n), \mathbf{t}_n, \theta, \mathbf{v}_n, v_\theta)$ and $(p_i^\downarrow(E_n), \mathbf{t}_n, \theta, \mathbf{v}_n, v_\theta)$ is

$$\frac{|v_i|}{2} \pi(p_i^\uparrow(E_n), \mathbf{t}_n, \theta, \mathbf{v}_n, v_\theta) + \frac{|v_i|}{2} \pi(p_i^\downarrow(E_n), \mathbf{t}_n, \theta, \mathbf{v}_n, v_\theta),$$

where the factors of $1/2$ are probabilities that a trajectory hitting the boundary from, say, $p_i^\uparrow(E_n)$ crosses into E_n rather than $p_i^\downarrow(E_n)$. The flow out of $(E_n, \mathbf{t}_n, \theta, \mathbf{v}_n, v_\theta)$ is $|v_i| \pi(E_n, \mathbf{t}_n, \theta, \mathbf{v}_n, v_\theta)$, and continuity of π implies zero net flux.

Finally, π is stationary at accessible type 1 boundaries because the flow of probability into state $(E_n, \mathbf{t}_n, \theta, \mathbf{v}_n, v_\theta)$ with $t_1 = 0+$ and $v_1 > 0$ is $v_1 \partial_1 \pi(E_n, \mathbf{t}_n, \theta, F_1 \mathbf{v}_n, v_\theta)$ —the rate with which probability mass hits the $t_1 = 0$ boundary due to the deterministic dynamics—which coincides with the flow out of $\pi(E_n, \mathbf{t}_n, \theta, F_1 \mathbf{v}_n, v_\theta)$, resulting in zero net flux. The same fact holds for the $\theta = 0$ boundary if there are no mutations. \square

We compared the zig-zag process to a Metropolis–Hastings algorithm by reanalyzing the data of [WFDP91] with $n = 55$, 14 distinct types, and 18 mutations. We used the improper prior $\pi_0(\theta) \propto \mathbf{1}_{(0, \infty)}(\theta)$, set $v_i = \pm 2/[(n+1-i)(n-i)]$, and set v_θ from trial runs to cross the θ -mode in unit time. The Supplementary Material details the Metropolis–Hastings algorithm and other tuning parameters in Table 3. We compared both methods to a hybrid combining zig-zag dynamics with continuous time Metropolis–Hastings moves at rate $\kappa = 10$. Performance was insensitive to κ provided it was not extreme: small values result in a zig-zag process, while large values result in Metropolis–Hastings.

Figure 4 shows that the zig-zag and hybrid methods mix visibly better than Metropolis–Hastings over the latent tree, as measured by the tree height $H_n := t_1 + \dots + t_{n-1}$. However, they are

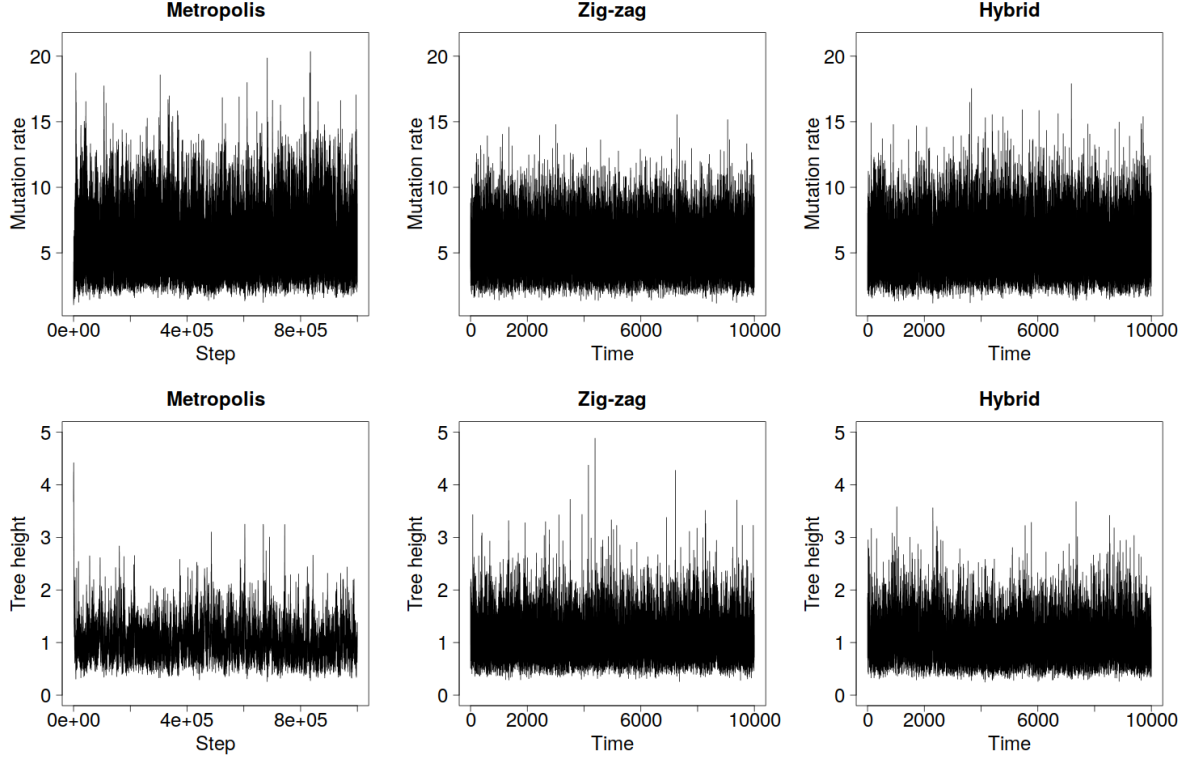


Figure 4: Trace plots under the infinite sites model and the data set of [WFDP91].

not as effective at exploring the upper tail of the θ -marginal, likely because they do not stay in regions of short trees for long enough for θ to increase into the tail.

To assess scaling, we simulated two data sets: one of size $n = 550$ with mutation rate $\theta = 5.5$ (the approximate posterior mean in Figure 4) and one with $n = 55$ and $\theta = 55$, which models a segment of DNA 10 times longer. Figures 5 and 6 demonstrate that the zig-zag and hybrid processes scale far better than Metropolis–Hastings, particularly when $\theta = 55$. Estimates in Table 1 quantify the improvement to 1–3 orders of magnitude.

Data set	Method	ESS(θ)/sec	ESS(H_n)/sec	Run time (min)
[WFDP91]	Metropolis	5	3	3.5
	Zig-zag	160	179	0.5
	Hybrid	128	67	0.5
$n = 550, \theta = 5.5$	Metropolis	0.1*	0.002*	70
	Zig-zag	1.7	1.2	45
	Hybrid	0.5	0.3	115
$n = 55, \theta = 55$	Metropolis	0.1*	0.1*	50
	Zig-zag	36	37	1
	Hybrid	22	22	1.5

Table 1: Effective sample sizes and run times for all three methods and data sets. Estimates were computed using the `ess` method of [FHVD17] under default settings for Metropolis–Hastings, and as in [BFR19a, Section 2] for the zig-zag and hybrid methods. Stars highlight poorly mixing chains with unreliable ESS estimates.

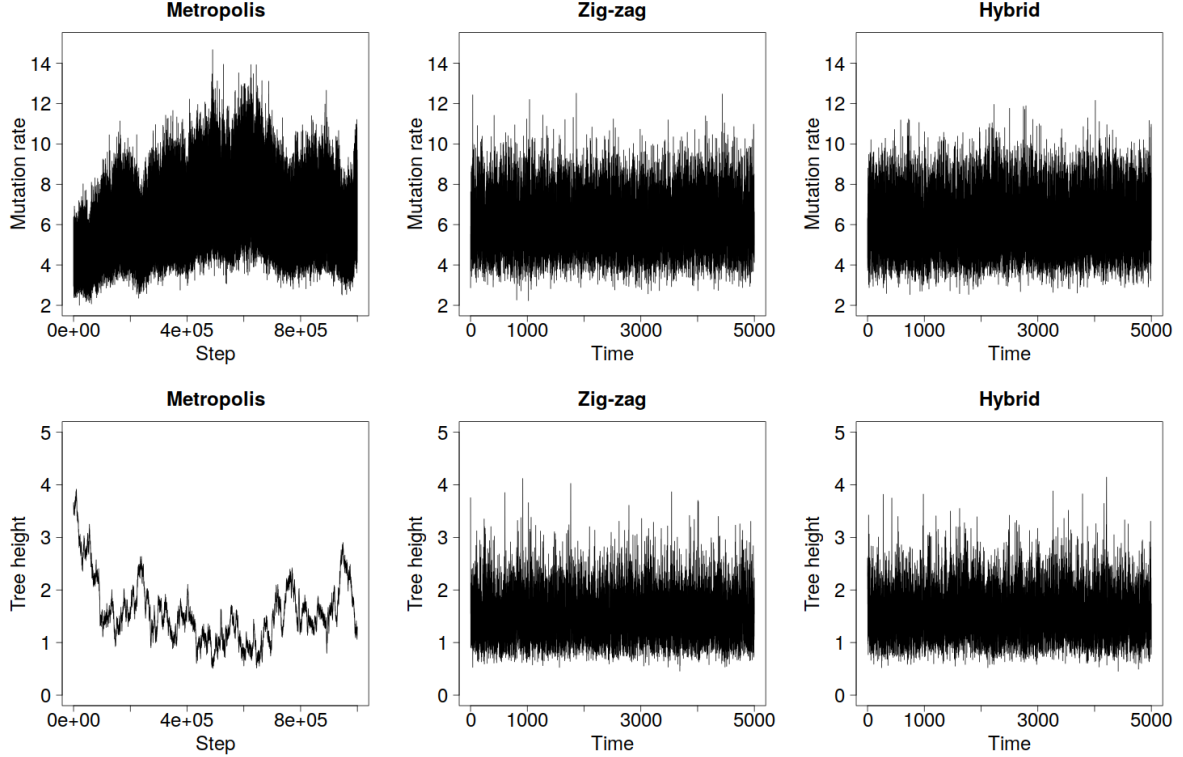


Figure 5: Trace plots for the infinite sites model and the data set with $n = 550$, $\theta = 5.5$, 30 distinct types, and 38 mutations.

4 The finite sites model

The finite sites model [JC69] is more detailed than the infinite sites model, but has greater computational cost. Consider a finite set of sites S with a finite number of possible types H per site; for example $H = \{0, 1\}$ or $H = \{A, T, C, G\}$. Mutations occur at each site with rate $\theta/(2|S|)$ and the type of a mutant child is drawn from stochastic matrix P with unique stationary distribution ν . We denote the transition matrix of the H -valued compound Poisson process with jump rate $\theta/(2|S|)$ and jump transition matrix P by $(Q_{hg}^\theta(t))_{h,g \in H; t \geq 0}$. Extensions to richer parameters or types are neglected for ease of presentation. Figure 7 depicts a realization of a finite sites coalescent.

The finite sites posterior can be written as a sum over the types of internal nodes:

$$\pi(E_n, \mathbf{t}_n, \theta) \propto \left\{ \prod_{s \in S} \sum_{\substack{h(s, c_\gamma) \in H \\ \text{for } \gamma \in F_n: |c_\gamma| > 1}} \prod_{\gamma \in F_n} Q_{h(s; p_\gamma)h(s; c_\gamma)}^\theta(t_\gamma) \right\} \times \exp \left(- \sum_{i=1}^{n-1} \binom{n+1-i}{2} t_i \right) \pi_0(\theta), \quad (6)$$

where $h(s; \eta) \in H$ is the type at site $s \in S$ on the node with label $\eta \in E_n$, and $\gamma \in F_n : |c_\gamma| > 1$ denotes edges which do not end in a leaf. The target (6) can be evaluated efficiently using the pruning algorithm of [Fel81]. Velocity flip rates can be written in terms of branch-specific

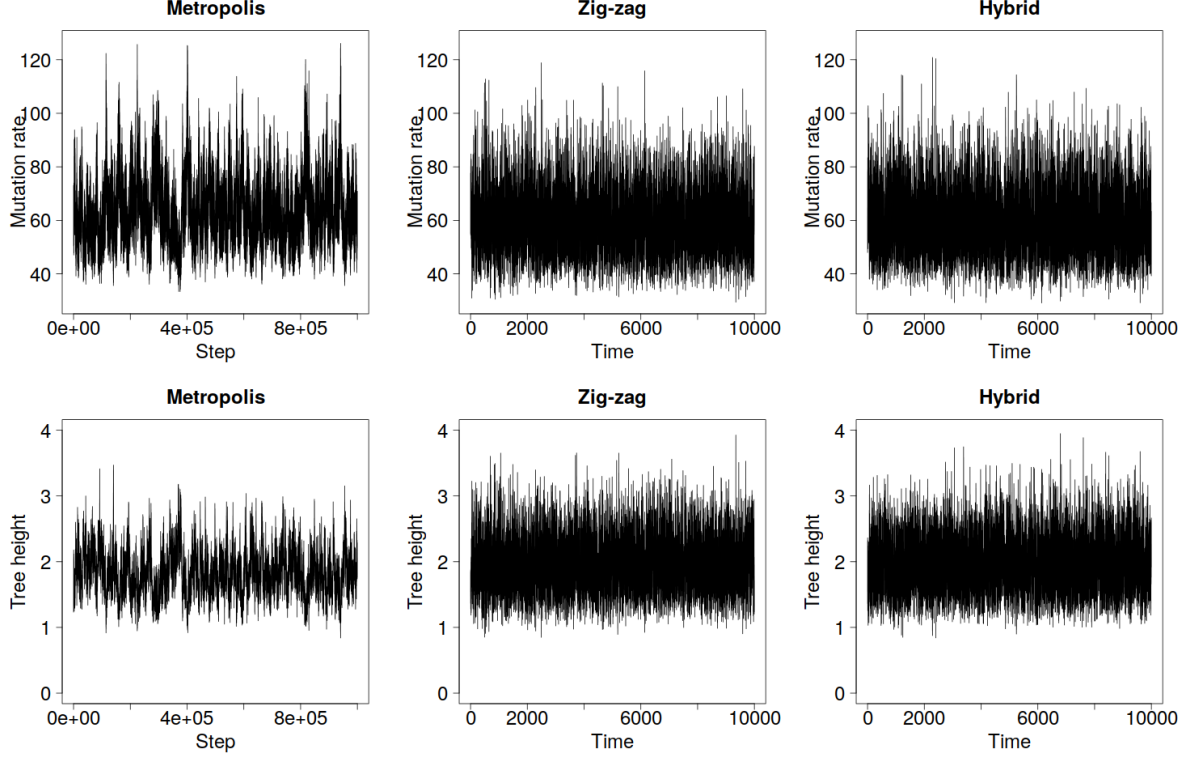


Figure 6: Trace plots for the infinite sites model and the data set with $n = 55$, $\theta = 55$, 40 distinct types, and 252 mutations.

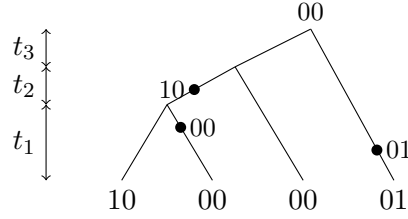


Figure 7: A realization of the finite sites model with $n = 4$, $S = H = \{0, 1\}$, three mutations, and three types. Note that the same type may arise many times.

gradients as

$$\lambda_i(E_n, \mathbf{t}_n, \theta; \mathbf{v}_n, v_\theta) = \left[v_i \left(\binom{n+1-i}{2} - \sum_{s \in S} \sum_{\substack{h(s, c_\gamma) \in H \\ \text{for } \gamma \in F_n: |c_\gamma| > 1}} \sum_{\delta \in F_n: t_i \in \delta} \frac{[\partial_i Q_{h(s; p_\delta)h(s; c_\delta)}^\theta(l_\delta)] \prod_{\gamma \in F_n: \gamma \neq \delta} Q_{h(s; p_\gamma)h(s; c_\gamma)}^\theta(l_\gamma)}{\sum_{\substack{h(s, c_\gamma) \in H \\ \text{for } \gamma \in F_n: |c_\gamma| > 1}} \prod_{\gamma \in F_n} Q_{h(s; p_\gamma)h(s; c_\gamma)}^\theta(l_\gamma)} \right) \right]^+, \quad (7)$$

$$\lambda_\theta(E_n, \mathbf{t}_n, \theta; \mathbf{v}_n, v_\theta) = \left[-v_\theta \left(\partial_\theta \log(\pi_0(\theta)) + \sum_{s \in S} \sum_{\substack{h(s, c_\gamma) \in H \\ \text{for } \gamma \in F_n: |c_\gamma| > 1}} \sum_{\delta \in F_n} \frac{[\partial_\theta Q_{h(s; p_\delta)h(s; c_\delta)}^\theta(l_\delta)] \prod_{\gamma \in F_n: \gamma \neq \delta} Q_{h(s; p_\gamma)h(s; c_\gamma)}^\theta(l_\gamma)}{\sum_{\substack{h(s, c_\gamma) \in H \\ \text{for } \gamma \in F_n: |c_\gamma| > 1}} \prod_{\gamma \in F_n} Q_{h(s; p_\gamma)h(s; c_\gamma)}^\theta(l_\gamma)} \right) \right]^+, \quad (8)$$

which can be evaluated using the linear-cost method of [JZH⁺20].

We show that events with rates (7) and (8) can be simulated using the example of [GT94, Section 7.4], in which $S = \{1, \dots, 20\}$, $H = \{0, 1\}$, and P is the 2×2 matrix which always changes state, corresponding to $\nu = (1/2, 1/2)$ and

$$Q_{hg}^\theta(t) := \frac{1}{2} + \left(\mathbb{1}_{\{h\}}(g) - \frac{1}{2} \right) e^{-\theta t}. \quad (9)$$

That (9) is not bounded away from 0 when $h \neq g$ means (7) and (8) lack simple bounds for Poisson thinning. As in Section 3, bounds can be obtained by time localization using

$$T \equiv T(E_n, \mathbf{t}_n, \theta; \mathbf{v}_n, v) := \min_{i \in \{1, \dots, n-1, \theta\}: v_i < 0} \left\{ \frac{-t_i}{[1 + c \mathbb{1}_{\{1, \theta\}}(i) \mathbb{1}_{\mathbb{Z}_+}(m_\gamma(E_n, i))] v_i} \right\}.$$

The variable T localizes the next zig-zag time step beginning at time t so that at most one branch can shrink to length zero on $[t, t + T]$, θ can fall by at most $1/(1 + c)$ of its present value, and t_1 can fall by at most $1/(1 + c)$ of its present value if the first two leaves to merge are of distinct types. This treatment of θ and t_1 is needed as (7) and (8) diverge in these cases, rendering the $\theta = 0$ and $t_1 = 0$ boundaries inaccessible.

Given $T \in (0, \infty)$, we have the following bounds on (9) on the time interval $[t, t + T]$:

$$\begin{aligned} Q_{hh}^\theta(l_\gamma) &\leq \frac{1}{2} \{1 + \exp(-[\theta + (v_\theta T)^-][l_\gamma + (v_\gamma T)^-])\}, \\ Q_{hg}^\theta(l_\gamma) &\leq \frac{1}{2} \{1 - \exp(-[\theta + (v_\theta T)^+][l_\gamma + (v_\gamma T)^+])\}, \\ Q_{hh}^\theta(l_\gamma) &\geq \frac{1}{2} \{1 + \exp(-[\theta + (v_\theta T)^+][l_\gamma + (v_\gamma T)^+])\}, \\ Q_{hg}^\theta(l_\gamma) &\geq \frac{1}{2} \{1 - \exp(-[\theta + (v_\theta T)^-][l_\gamma + (v_\gamma T)^-])\}, \end{aligned}$$

for $h \neq g$. Substituting these bounds into [JZH⁺20, Equation (9)] provides bounds on flip rates that can be evaluated with $O(|S|n)$ cost.

Figure 8 demonstrates that the zig-zag process again mixes over latent trees faster than Metropolis–Hastings, but struggles to explore the upper tail of the θ -marginal. The hybrid method was run with $\kappa = 100$ to account for shorter run lengths than in Section 3, and thus resembles Metropolis–Hastings rather than the zig-zag process.

Figures 9 and 10 show results for two further simulated data sets: one with $n = 200$ and $S = 20$, and one with $n = 50$ and $S = 200$. The superior mixing of the zig-zag process over the latent tree is clear. The lack of mixing in the upper tail of the θ -marginal is also stark, particularly in Figure 9 where zig-zag significantly underestimates posterior variance. The estimated posterior means of all three methods coincide in all cases (results not shown).

5 Zig-zag for general discrete targets

The zig-zag methods in Sections 3 and 4 were model-specific, but can be generalized. Consider a target $\pi(m, \mathbf{x}) > 0$ supported on $\mathbb{F} \times \Omega \subset \mathbb{N} \times \mathbb{R}^d$ for $d \geq 1$. The model-specific part of the construction is arranging $|\mathbb{F}|$ copies of Ω into a connected space $\Omega^\mathbb{F} := \cup_{i \in \mathbb{F}} \Omega_i$ such that intersections $\Omega_i \cap \Omega_j$ are piecewise smooth, $(d - 1)$ -dimensional manifolds which contain no interior points of any $\Omega_i \in \Omega^\mathbb{F}$, and only a bounded number of sets $\{\Omega_i\}_{i \in \mathbb{F}}$ intersect at any point. We define $B^\mathbb{F} := \cup_{i \neq j \in \mathbb{F}} \{\Omega_i \cap \Omega_j\}$ and $I^\mathbb{F} := \Omega^\mathbb{F} \setminus B^\mathbb{F}$.

For $\mathbf{y} \in I^\mathbb{F}$, let $m(\mathbf{y})$ be the index of the copy $\Omega_{m(\mathbf{y})}$ containing \mathbf{y} , and $x(\mathbf{y}) : \Omega^\mathbb{F} \rightarrow \Omega$ be the projection that forgets $m(\mathbf{y})$. Consider state space $\mathbb{F} \times \Omega^\mathbb{F} \times \{-1, 1\}^d$ and define $\tilde{\pi}(m, \mathbf{y}, \mathbf{v}) :=$

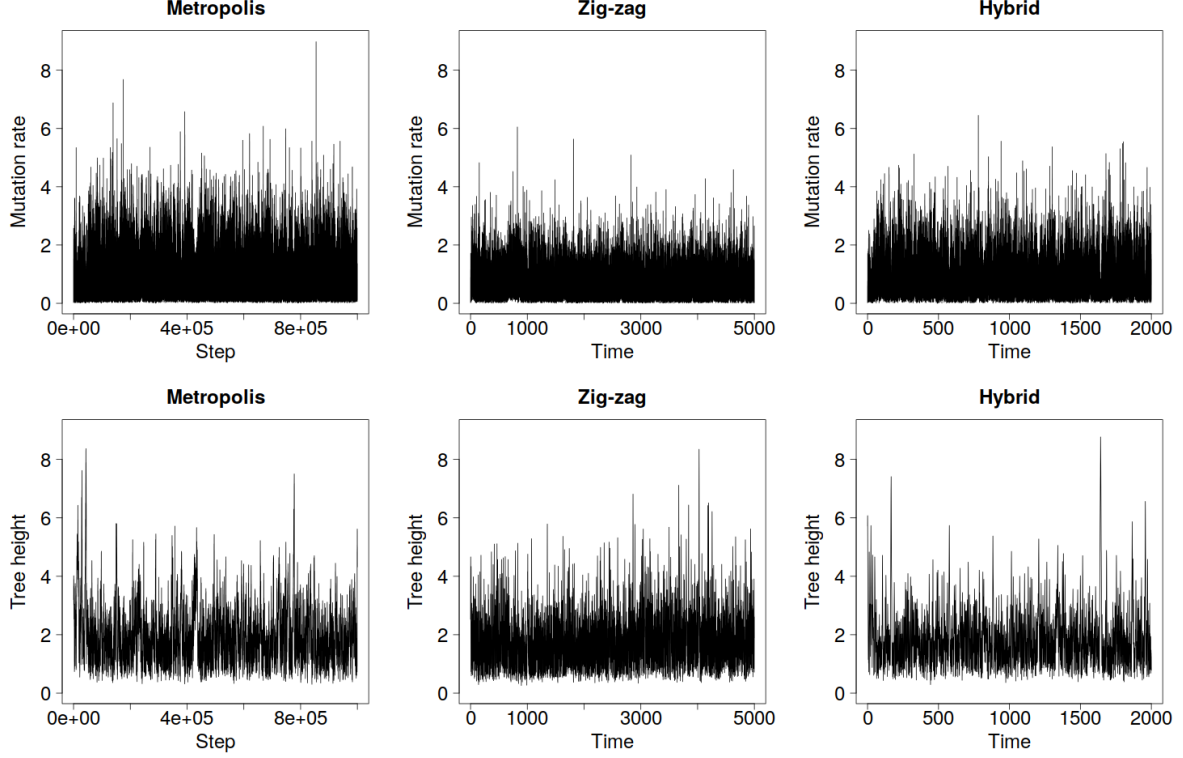


Figure 8: Trace plots for the finite sites model and data from [GT94].

$\mathbb{1}_{\{m\}}(m(\mathbf{y}))\pi(m, m(\mathbf{y}), x(\mathbf{y}))/2^d$. Tracking the occupancy index m separately from $m(\mathbf{y})$ is redundant when $\mathbf{y} \in I^{\mathbb{F}}$, but helpful when $\mathbf{y} \in B^{\mathbb{F}}$. Taking $\Omega = \mathbb{R}_+^d$ and $B^{\mathbb{F}} = \{\mathbf{y} \in \Omega^{\mathbb{F}} : y_i = 0 \text{ for some } i \in \{1, \dots, d\}\}$ is a natural example.

At points $(m, \mathbf{y}, \mathbf{v}) \in \mathbb{F} \times I^{\mathbb{F}} \times \{-1, 1\}^d$, the usual zig-zag dynamics acting on $\mathbf{y} \in I^{\mathbb{F}}$ via velocities $\mathbf{v} \in \{-1, 1\}^d$ targeting $\tilde{\pi}$ solve a Fokker–Planck equation akin to (5) provided velocity flip rates are bounded on compact subsets of $\mathbb{F} \times \Omega^{\mathbb{F}} \times \{-1, 1\}^d$. It remains to construct boundary crossings which ensure zero net probability flux across $B^{\mathbb{F}}$. Proposition 2 provides sufficient conditions which generalize the processes of Sections 3 and 4.

Proposition 2. *Consider a zig-zag process on $\mathbb{F} \times \Omega^{\mathbb{F}} \times \{-1, 1\}^d$ targeting $\tilde{\pi}$ as described above with $\Omega = \mathbb{R}_+^d$ and $B^{\mathbb{F}} := \{\mathbf{y} \in \Omega^{\mathbb{F}} : y_i = 0 \text{ for some } i \in \{1, \dots, d\}\}$. Conditional on hitting $(m, \mathbf{y}, \mathbf{v}) \in \mathbb{F} \times (\Omega_m \cap B^{\mathbb{F}}) \times \{-1, 1\}^d$ at time $t \rightarrow 0$ with $y_i = 0$ and $v_i < 0$, let the state at time t be $(M, \mathbf{y}, F_i \mathbf{v})$ where $i \in \{1, \dots, d\}$ is the index of the coordinate in which the boundary was hit, and M is an \mathbb{F} -valued random variable. If the conditional law of $M|(m, \mathbf{y})$ satisfies*

$$[1 - \mathbb{P}(M = m|m, \mathbf{y})]\tilde{\pi}(m, \mathbf{y}, \mathbf{v}) = \sum_{m' \neq m: \mathbf{y} \in \Omega_{m'} \cap \Omega_m} \mathbb{P}(M = m'|m', \mathbf{y})\tilde{\pi}(m', \mathbf{y}, \mathbf{v}) \quad (10)$$

for $\tilde{\pi}$ -a.e. $(m, \mathbf{y}, \mathbf{v}) \in \mathbb{F} \times B^{\mathbb{F}} \times \{-1, 1\}^d$, then the net probability flux across $B^{\mathbb{F}}$ is zero.

Proof. When the zig-zag process has initial distribution $\tilde{\pi}$, the right-hand side of (10) is the flow of probability into state $(m, \mathbf{y}, F_i \mathbf{v})$ from states $\cup_{m' \neq m: \mathbf{y} \in \Omega_{m'} \cap \Omega_m} (m', \mathbf{y}, \mathbf{v})$. The left-hand side is the flow out of $(m, \mathbf{y}, \mathbf{v})$. By construction, $\tilde{\pi}(m, \mathbf{y}, \mathbf{v}) = \tilde{\pi}(m, \mathbf{y}, F_i \mathbf{v})$ so that net probability flux is zero. \square

If $\tilde{\pi}(m(\mathbf{y}), \mathbf{y}, \mathbf{v})$ is continuous in $\mathbf{y} \in \Omega^{\mathbb{F}}$, then $M|(m, \mathbf{y}) \sim U(\{m' \neq m : \mathbf{y} \in \Omega_{m'} \cap \Omega_m\})$ solves (10). Discontinuous targets can be handled using reflections back into Ω_m as in HMC [NDL20].

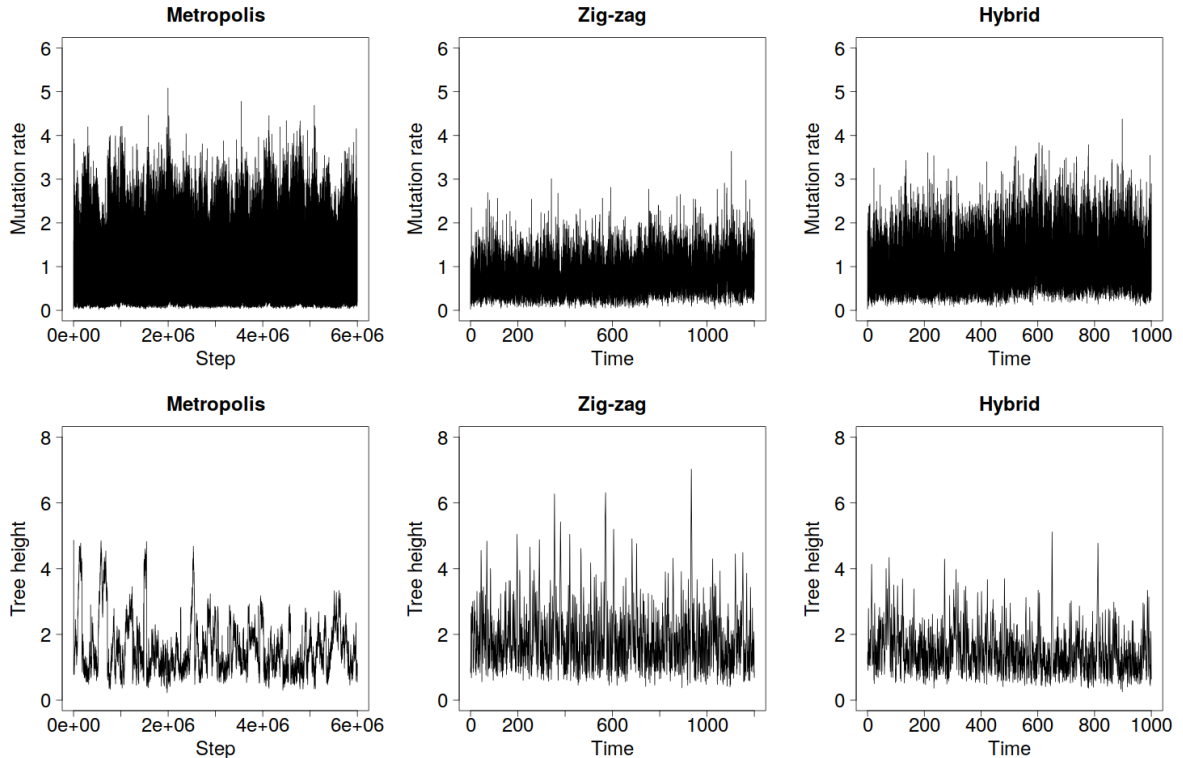


Figure 9: Trace plots for the finite sites model and data set with $n = 500$ and $S = 20$ consisting of five distinct sequences.

[CFS20] provide a similar construction for model selection, in which the sets Ω_i are nested, and for $j < i$, the boundary $\Gamma_{i,j}$ lies in the interior of Ω_i . They provide similar conditions for balancing probability fluxes [CFS20, Section 4.1], but their approach seems difficult to adapt to settings in which discrete variables lack a partial order. [GD20] also consider model selection on nested spaces, and use an accept-reject mechanism [GD20, Equation (2)] to ensure zero net probability flux.

6 Discussion

The coalescent is a gold-standard model in phylogenetics, but its practical use is hindered by slow mixing of MCMC methods over latent trees [MV05, HDPD08, LVH⁺08]. We have constructed a zig-zag process for the coalescent and shown that it can improve mixing over trees, particularly under the infinite sites model. This model is widely used to analyze ever larger data sets, and the zig-zag process shows promise for expanding the scope of feasible MCMC computations.

The zig-zag process was more efficient than Metropolis–Hastings under the infinite sites model in terms of effective sample size, but struggled to explore the tails of the θ -marginal. A likely reason is correlation in the target: high mutation rates are only be attainable when branch lengths are short. A Metropolis–Hastings algorithm can jump to a high mutation rate as soon as the latent tree has short branches, while the zig-zag process must traverse all intervening mutation rates before branch lengths grow. The hybrid method with both types of motion interpolated between the zig-zag and Metropolis–Hastings algorithms.

The finite sites model required much higher run times from all three algorithms. Estimated effective sample sizes in Table 2 distinguish the methods only weakly: zig-zag is superior to Metropolis–Hastings in some cases, but worse at estimating θ when $n = 500$. Trace plots tell the same story as for the infinite sites model: zig-zag shows superior mixing over latent trees,

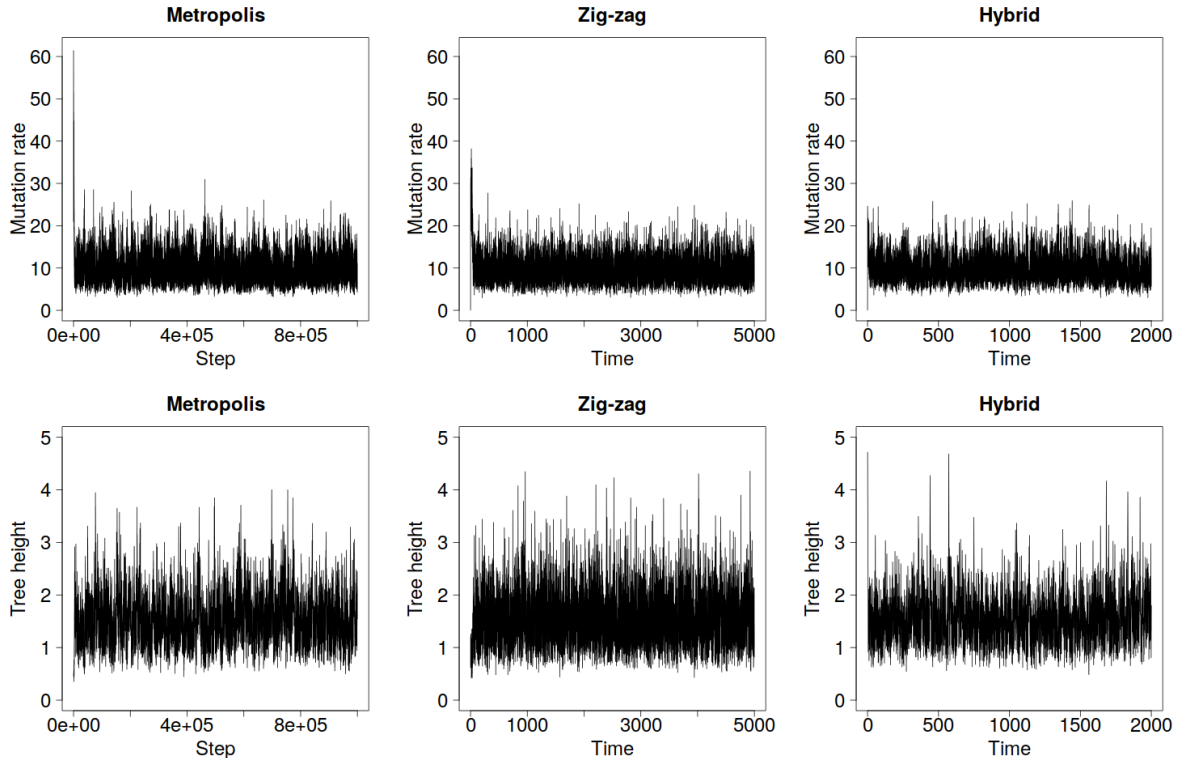


Figure 10: Trace plots for the finite sites model and data set with $n = 50$ and $S = 200$ consisting of 18 distinct sequences.

but struggles to explore the upper tail of the θ -marginal, particularly when $n = 500$ where it markedly underestimates posterior variance of θ .

The long run times of the zig-zag and hybrid methods for the finite sites model are due to the $O(|S|n)$ cost per evaluation of (7) and (8). There are also $O(n)$ velocities for which to simulate flip times. However, flip times across velocities are conditionally independent given the current state and can be generated in parallel, unlike steps of the Metropolis–Hastings algorithm. Thus, the zig-zag process is well suited to parallel architectures.

Our work is the first non-reversible MCMC method for the coalescent and contributes to gradient-based methods for discrete targets. We show that zig-zag processes can sample discrete variables embedded into continuous space [DBZM17, NDL20], sometimes more simply than HMC (though see [NDL20, Section S6.4]). Sections 3 and 4 demonstrate coalescent constructions, while Section 5 provides a generic scheme assuming that a model-specific embedding is available.

The key to the coalescent zig-zag process was τ -space [GD16], which enabled the sampling of discrete tree topologies using piecewise deterministic Markov processes with continuous paths, and the defining of gradients of a target with discrete components. While τ -space is convenient for ultrametric trees, it is not unique: [GD16] also present a second embedding called t -space. Good choices of embedding are likely to be problem-specific, but crucial for good performance. For example, both τ -space and t -space would be awkward for non-contemporaneous data.

It is natural to ask whether non-reversible methods can yield similar improvements in population genomics, where different regions of DNA have different but correlated ancestries due to e.g. crossover recombination. Here the standard model is the ancestral recombination graph (ARG) [Hud90] in which ancestral trees are embedded into a common graph that is not itself a tree. The ARG is an even more challenging model for MCMC than the coalescent due to its larger and vari-

Data set	Method	ESS(θ)/sec	ESS(H_n)/sec	Run time (min)
[GT94]	Metropolis	1.8	0.2	29
	Zig-zag	2.3	1.0	18
	Hybrid	2.1	0.6	16
$n = 500, S = 20$	Metropolis	0.09	0.0006*	1567
	Zig-zag	0.01*	0.004	1749
	Hybrid	0.01	0.003	1800
$n = 50, S = 200$	Metropolis	0.04	0.03	257
	Zig-zag	0.05	0.13	175
	Hybrid	0.08	0.07	183

Table 2: Effective sample sizes and run times for all three methods and data sets. Estimates were computed as in Table 1. Stars highlight unmixed chains with unreliable ESS estimates.

able dimensionality. Reversibility is also a major obstacle for implementing Metropolis–Hastings samplers for the ARG. Local rearrangement of edges near the leaves can render large regions of the graph non-ancestral to the sample, at which point storing them is an unnecessary (and at worst exponentially large) overhead. Deleting redundant regions cannot be done reversibly without a positive probability of simulating them in a reverse move [KYF00, Implementation], which complicates the design of Metropolis–Hastings proposals. A non-reversible method could in principle delete redundant regions as they appear, and thus avoid this complication entirely.

SUPPLEMENTARY MATERIAL

This supplement details the Metropolis–Hastings algorithms used in Sections 3 and 4. Both used the same proposal mechanisms consisting of three steps. An iteration of the algorithm is one scan through all three steps, with an accept/reject correction after each step. The hybrid method only used steps 1 and 3.

1. A Gaussian random walk update of θ reflected at 0 with proposal variance σ_θ^2 tuned to obtain an average acceptance probability $\alpha_\theta \approx 1/4$.
2. An update of holding times \mathbf{t}_n under a fixed topology.
3. A subtree-prune-regraft step.

Type 2 updates first additively perturb the initial holding time t_1 as

$$\xi_1 \sim \mathcal{N}(t_1, \sigma_{\mathbf{t}_n}^2 / [n(n-1)^2]) | \xi_1 > 0.$$

Further holding times $i \in \{2, \dots, n-1\}$ are conditionally independently perturbed as

$$\xi_i | (\xi_1, \dots, \xi_{i-1}) \sim \mathcal{N}(t_i, \sigma_{\mathbf{t}_n}^2 / [(n-1)(n-i+1)(n-i)]) | \xi_i > \xi_{c_{i,1}} \vee \xi_{c_{i,2}},$$

where $\xi_{c_{i,1}}$ and $\xi_{c_{i,2}}$ are the perturbed times of the child nodes of the node at time t_i . Again, $\sigma_{\mathbf{t}_n}$ was tuned so that the average acceptance probability was $\alpha_{\mathbf{t}_n} \approx 1/4$.

Type 3 updates sample an ordered pair of edges $(\gamma, \gamma') \sim U(F_n \times [F_n \cup \gamma_{MRCA}])$, where γ_{MRCA} is an edge connecting the MRCA to ∞ . Edge γ is deleted, and its child c_γ is reattached into γ' . Letting t_η be the time of the node with label $\eta \in E_n$ in an abuse of notation, the reattachment time t' has distribution

$$t' \sim U(t_{c_\gamma} \wedge t_{c_{\gamma'}}, t_{p_{\gamma'}}) \text{ if } \gamma' \neq \gamma_{MRCA},$$

$$t' - t_{c_{\gamma_{MRCA}}} \sim \text{Exp}(1) \text{ otherwise.}$$

Under the infinite sites model, moves into topologies incompatible with observed mutations were rejected essentially instantaneously, without costly likelihood evaluations.

Table 3 summarizes hyperparameters and quantities of interest used in the simulation.

Data set	Method	v_θ	σ_θ	σ_{t_n}	α_θ	α_{t_n}	α_{SPR}	κ
[WFDP91]	Metropolis	-	8	0.6	0.27	0.25	0.06	-
	Zig-zag	8	-	-	-	-	-	-
	Hybrid	8	10	-	0.24	-	0.06	10
$n = 550, \theta = 5.5$	Metropolis	-	6	0.25	0.23	0.24	0.03	-
	Zig-zag	6	-	-	-	-	-	-
	Hybrid	6	6	-	0.23	-	0.03	10
$n = 55, \theta = 55$	Metropolis	-	18	0.4	0.26	0.23	0.02	-
	Zig-zag	40	-	-	-	-	-	-
	Hybrid	40	18	-	0.24	-	0.01	10
[GT94]	Metropolis	-	4	0.7	0.23	0.25	0.12	-
	Zig-zag	4	-	-	-	-	-	-
	Hybrid	4	4	-	0.24	-	0.12	100
$n = 500, S = 20$	Metropolis	-	4	0.3	0.21	0.21	0.31	-
	Zig-zag	4	-	-	-	-	-	-
	Hybrid	4	3	-	0.29	-	0.32	100
$n = 50, S = 200$	Metropolis	-	14	0.6	0.20	0.27	0.04	-
	Zig-zag	20	-	-	-	-	-	-
	Hybrid	20	14	-	0.20	-	0.04	100

Table 3: Hyperparameters and acceptance probabilities for simulations in sections 3 and 4.

References

- [ASR16] A. J. Aberer, A. Stamatakis, and F. Ronquist. An efficient independence sampler for updating branches in Bayesian Markov chain Monte Carlo sampling of phylogenetic trees. *Syst. Biol.*, 65(1):161–176, 2016.
- [BBCD⁺18] J. Bierkens, A. Bouchard-Côte, A. Doucet, A. B. Duncan, P. Fearnhead, T. Lienart, G. Roberts, and S. J. Vollmer. Piecewise deterministic Markov processes for scalable Monte Carlo on restricted domains. *Stat. Probab. Lett.*, 136:148–154, 2018.
- [BFR19a] J. Bierkens, P. Fearnhead, and G. Roberts. Supplement to the zig-zag process and super-efficient sampling for Bayesian analysis of big data. *Ann. Stat.*, 47, 2019.
- [BFR19b] J. Bierkens, P. Fearnhead, and G. Roberts. The zig-zag process and super-efficient sampling for Bayesian analysis of big data. *Ann. Stat.*, 47(3):1288–1320, 2019.
- [BHV01] L. J. Billera, S. P. Holmes, and K. Vogtmann. Geometry of the space of phylogenetic trees. *Adv. Appl. Math.*, 27:733–767, 2001.
- [BR17] J. Bierkens and G. Roberts. A piecewise deterministic scaling limit of lifted Metropolis-Hastings for the Curie-Weiss model. *Ann. Appl. Probab.*, 27(2):846–882, 2017.
- [CFS20] A. Chevalier, P. Fearnhead, and M. Sutton. Reversible jump PDMP samplers for variable selection. Preprint, arXiv:2010.11771, 2020+.
- [DBZM17] V. Dinh, A. Bilge, C. Zhang, and F. A. Matsen IV. Probabilistic path Hamiltonian Monte Carlo. In *Proceedings of the 34th International Conference on Machine Learning*, Sydney, Australia, 2017.
- [FBPR18] P. Fearnhead, J. Bierkens, M. Pollock, and G. Roberts. Piecewise deterministic Markov processes for continuous-time Monte Carlo. *Stat. Sci.*, 33(3):386–412, 2018.

- [Fel81] J. Felsenstein. Evolutionary trees from DNA sequences: a maximum likelihood approach. *J. Mol. Evol.*, 17:368–376, 1981.
- [FHVD17] J. M. Flegel, J. Hughes, D. Vats, and N. Dai. *mcmcse: Monte Carlo Standard Errors for MCMC*, 2017.
- [GD16] A. Gavryushkin and A. J. Drummond. The space of ultrametric phylogenetic trees. *J. Theor. Biol.*, 403:197–208, 2016.
- [GD20] P. Gagnon and A. Doucet. Nonreversible jump algorithms for Bayesian nested model selection. *J. Comput. Graph. Stat.*, 2020.
- [Gey92] C. J. Geyer. Practical Markov chain Monte Carlo. *Statist. Sci.*, 7:473–483, 1992.
- [GS90] A. E. Gelfand and A. F. M. Smith. Sampling-based approaches to calculating marginal densities. *J. Am. Stat. Assoc.*, 85(410):398–409, 1990.
- [GT94] R. C. Griffiths and S. Tavaré. Simulating probability distributions in the coalescent. *Theor. Popln Biol.*, 46:131–159, 1994.
- [Has70] W. K. Hastings. Monte Carlo sampling methods using Markov chains and their applications. *Biometrika*, 57:97–109, 1970.
- [HD12] S. Höhna and A. J. Drummond. Guided tree topology proposals for Bayesian phylogenetic inference. *Syst. Biol.*, 61(1):1–11, 2012.
- [HDPD08] S. Höhna, M. Defoin-Platel, and A. J. Drummond. Clock-constrained tree proposal operators in Bayesian phylogenetic inference. In *BioInformatics and BioEngineering*, pages 1–7, 8th IEEE International Conference on IEEE, 2008.
- [Hud90] R. R. Hudson. Gene genealogies and the coalescent process. In D. J. Futuyama and J. Antonovics, editors, *Oxford Surveys in Evolutionary Biology*. Oxford University Press, 1990.
- [JC69] T. H. Jukes and C. R. Cantor. Evolution of protein molecules. In H. N. Munro, editor, *Mammalian protein metabolism*, pages 21–132. Academic Press, New York, 1969.
- [JZH⁺20] X. Ji, Z. Zhang, A. Holbrook, A. Nishimura, G. Baele, A. Rambaut, P. Lemey, and M. A. Suchard. Gradients do grow on trees: a linear-time $O(N)$ -dimensional gradient for statistical phylogenetics. *Mol. Biol. Evol.*, 37(10):3047–3060, 2020.
- [Kin82] J. F. C. Kingman. The coalescent. *Stochast. Process. Applic.*, 13(3):235–248, 1982.
- [KYF00] M. K. Kuhner, J. Yamamoto, and J. Felsenstein. Maximum likelihood estimation of recombination rates from population data. *Genetics*, 156:1393–1401, 2000.
- [LVH⁺08] C. Lakner, P. Van Der Mark, J. P. Huelsenbeck, B. Larget, and F. Ronquist. Efficiency of Markov chain Monte Carlo tree proposals in Bayesian phylogenetics. *Syst. Biol.*, 57:86–103, 2008.
- [MV05] E. Mossel and E. Vigoda. Phylogenetic MCMC algorithms are misleading on mixtures of trees. *Science*, 309:2207–2209, 2005.
- [NDL20] A. Nishimura, D. B. Dunson, and J. Lu. Discontinuous Hamiltonian Monte Carlo for discrete parameters and discontinuous likelihoods. *Biometrika*, 107(2):365–380, 2020.
- [Nea10] R. M. Neal. MCMC using Hamiltonian dynamics. In *Handbook of Markov chain Monte Carlo*. CRC Press, 2010.

- [Wak09] J. Wakeley. *Coalescent theory: an introduction*. Roberts & Co, 2009.
- [Wat75] G. A. Watterson. On the number of segregating sites in genetical models without recombination. *Theor. Popln Biol.*, 7:256–276, 1975.
- [WFDP91] R. H. Ward, B. L. Frazier, K. Dew, and S. Pääbo. Extensive mitochondrial diversity within a single Amerindian tribe. *Proc. Natl. Acad. Sci. USA*, 88:8720–8724, 1991.